https://doi.org/10.5194/amt-2023-171
Preprint. Discussion started: 19 September 2023

Atmospheric Measurement Techniques Discussions
Open Access
EGU

Identifying the seeding signature in cloud particles from hydrometeor residuals

Mahen Konwar[1*], Benjamin Werden[2], Edward C. Fortner[2], Sudarsan Bera[1], Mercy Varghese[1], Subharthi Chowdhuri[1,&], Kurt Hibert[3], Philip Croteau[2], John Jayne[2], Manjula Canagaratna[2], Neelam Malap[1], Sandeep Jayakumar[1], Shivsai A. Dixit[1], Palani Murugavel[1], Duncan Axisa[4], Darrel Baumgardner[5], Peter F. DeCarlo[6], Doug R.Worsnop[2], and Thara Prabhakaran[1]

[1] Indian Institute of Tropical Meteorology, Ministry of Earth Sciences, Pune, India 411008

[2]Aerodyne Research Inc., Billerica, MA, USA, 01821

[3]Weather Modification Inc., Fargo, ND, USA, 58102

[4]Center for Western Weather and Water Extremes, Scripps Institution of Oceanography, La Jolla, CA 92037, USA

[5] Droplet Measurement Technologies, Longmont, CO, USA, 80503

[6]Department of Environmental Health and Engineering, Johns Hopkins University, Baltimore, MD USA 21218

[&]now at University of California, Irvine, CA 92697-2700, USA

*Corresponding author

Dr. Mahen Konwar

Indian Institute of Tropical Meteorology

Dr. Homi Bhabha Road, Pune 411 008, India.

Email: mkonwar@tropmet.res.in

https://doi.org/10.5194/amt-2023-171
Preprint. Discussion started: 19 September 2023

Atmospheric Measurement Techniques
Open Access
Discussions

Abstract:

Cloud seeding experiments for modifying cloud and precipitation have been underway for nearly a century; yet practically all the attempts to link precipitation enhancement or suppression to the presence of seeding materials remained inclusive. In 2019, the Cloud-Aerosol Interaction and Precipitation Enhancement Experiment (CAIPEEX) implemented a novel method to detect seeded clouds during its operations in Solapur, India. In this experiment, residuals of cloud hydrometeors in seeded and non-seeded clouds were analyzed with an airborne mini-Aerosol Mass Spectrometer (mAMS). The mAMS instrument was utilized in conjunction with a counterflow virtual impactor (CVI) inlet, which had a cutoff diameter size of approximately 7 µm. Upon traversing the CVI inlet, the cloud droplets underwent a drying process, enabling the subsequent examination of cloud residuals through the mAMS instrument to identify potential seeding signatures. The Chlorine (Cl) associated with hygroscopic materials, i.e., Calcium Chloride ($CaCl_2$) and potassium (K), which serve as the oxidizing agents in the flares, is found in relatively higher concentrations in the seeded clouds compared to the non-seeded clouds. After seeding, small-size cloud droplet concentrations increased in the convective and stratus clouds. In the convective clouds, flare particles propagated to higher cloud depths (≈ 2.25 km, vertical distance from cloud base) and modulate cloud microphysical properties to initiate warm rain. This new technique help to trace activated flare particles in seeded clouds and identify the post-seeding chain of cloud microphysical processes.

https://doi.org/10.5194/amt-2023-171
Preprint. Discussion started: 19 September 2023

Atmospheric Measurement Techniques Discussions

1. Introduction:

E.G. Bowen first proposed in 1952 that hygroscopic particles can foster collision-coalescence (CC) processes in a cloud (Bowen, 1952). Since then, cloud seeding experiments have been conducted worldwide to mitigate and manage the ever-increasing urban water demand during a drought season or in drought-prone regions. More than 50 countries are involved in weather modification projects (Flossmann, et al., 2019). Over the years, the interest in rain enhancement projects has increased due to the accumulating evidence of a potentially positive effect (i.e., enhancement in rainfall) in several seeding experiments (Mather et al., 1996; Mather et al. 1997; Bruintjes, 1999; WMO, 2000). However, skepticism remains within the broader cloud physics community because the efficacy of many cloud seeding experiments remains inconclusive (Ryan and King, 1997; Silverman, 2003). In addition to the existing challenge of evaluating the effectiveness of cloud seeding experiments, another pivotal longstanding issue revolves around accurately detecting the hygroscopic particles released within a cloud, identifying the seeded cloud, and comprehending the impact of seeding on the cloud microphysical properties.

Traditionally, in a cloud seeding experiment tracers such as the inert gas, sulfur hexafluoride (SF_6) (Rosenfeld et al., 2010; Stith, et al., 1986; Stith et al., 1990; Bruintjes et al., 1995), or radar chaff at cloud bases are released and then these traces are tried to measure higher in the cloud. However, successful tracing of SF_6 in a seeded cloud is challenging and reported only on a few occasions near the cloud base (Rosenfeld et al., 2010). The tracers used in various experiments have certain limitations, such as their detection limit and the presence of high background concentrations, as seen in tracers like SF_6. Consequently, several questions arise during these experiments. For instance, does the dispersed seeding material effectively enter the targeted cloud region? Up to what altitude do these materials reach? Are the in-situ measurements being conducted within the intended

https://doi.org/10.5194/amt-2023-171
Preprint. Discussion started: 19 September 2023

cloud volume? How can transported flare particles be located within large clouds? It is important to note that SF_6 is a potent greenhouse gas, with the highest radiative efficiencies of any molecule (Ravishankara et al., 1993, Hodnebrog et al., 2013) and is stable with an atmospheric lifetime of 850 years with an uncertainty range of 580–1400 years (Ray et al., 2017). Therefore, the release of SF_6 in cloud seeding experiments has the detrimental effect of adding more greenhouse gases to the atmosphere and is a burden to the Earth's atmosphere. Due to the uncertainty and side effects of the tracing materials, the development of a low-impact but similarly effective tracer was suggested (Tessendorf et al., 2012).

A critical question in any cloud seeding experiment is whether the observed changes in the cloud microphysical properties after seeding are due to the seeding effect or to natural cloud processes. There are two requirements necessary to address this question: (i) Can the trajectory of seeding material be successfully traced in the cloud, and (ii) can changes in cloud microphysical processing be linked to seeding materials? In this study, an instrumented aircraft was deployed to acquire convincing evidence of seeding chemicals inside clouds and the plausible chain of microphysical processes caused by these seeding materials. This work primarily addresses how to trace seed particles' signatures in clouds. This novel technique uses a mini-Aerosol Mass Spectrometer (mAMS) (Jayne et al., 2000) behind a counterflow virtual impactor (CVI) inlet (Noone et al., 1988; Shingler et al., 2012) to identify seeding material in the residual cloud droplets.

The hygroscopic cloud seeding hypothesis relies on a chain of microphysical mechanisms. Dispersal of giant cloud condensation nuclei (CCN), hygroscopic particles with diameter, D, between 1-10 μm, in the updraft region of a cloud base adds larger drops to the tail of the natural cloud droplet size distribution (DSD), known as the 'tail effect.' This effect further accelerates the formation of raindrops through CC (Segal et al., 2004; Segal, et al., 2007; Kuba and Murakami,

https://doi.org/10.5194/amt-2023-171
Preprint. Discussion started: 19 September 2023

2010; Konwar et al, 2023). With the initial activation and growth of these larger CCNs, the supersaturation over water droplets (SS_w) decreases above the cloud base. As a result, the smaller, natural CCN does not activate. This effect reduces the total droplet number concentration (N_t, cm^{-3}) and broadens the DSDs, known as the 'competition effect.' This broadening fosters the droplet growth rate by intensifying the CC process, which accelerates the formation of precipitation (Cooper et al., 1997; Rosenfeld et al., 2010). Past studies examined well-formed seeded clouds, with in-situ measurements observing the broadening of DSDs by hygroscopic seeding in marine stratocumulus clouds (Ghate et al., 2007). Researchers reported that an increased concentration of small cloud droplets occurred at an earlier stage, while at a later stage, an increased concentration in the large D range of 20-40 μm was noted. In another study, the tracer SF_6 was used to track a seeded cloud, where milled salt particles were used as the seed, and the broadening of DSD was observed (Rosenfeld et al., 2010). Observations of glaciogenic seeding experiments (French et al., 2018) have illustrated physical seeding signatures. Linking the evolution of cloud microphysical processes to hygroscopic seeding remains elusive despite worldwide hygroscopic cloud seeding experiments (Flossmann et al., 2019; Silverman 2003; Tessendorf et al., 2012). The major hurdle is that the physical processes leading to precipitation formation are dynamic and complex and difficult to accurately track and link to the seeding (Tessendorf et al., 2012).

In the current study, using an mAMS, we demonstrate that the seeding signatures within stratus and convective clouds are detectable with an evidence-based approach without using tracer gasses. We further show that the seeding materials and the seeding-activated cloud droplets in convective clouds can propagate to higher altitudes while also modulating the cloud's microphysical properties. The ultimate goal is to investigate the microphysical pathways that are modified in cloud seeding operations. These experiments took place in the region near Solapur (17.66° N, 75.90° E),

https://doi.org/10.5194/amt-2023-171
Preprint. Discussion started: 19 September 2023

Atmospheric Measurement Techniques Discussions

India, during the Cloud-Aerosol Interaction and Precipitation Enhancement Experiment (CAIPEEX) (Prabha et al., 2011; Kulkarni et al., 2012) in 2019 (phase-IV).

2. Materials and Methods:

2.1 Measurements of cloud properties.

Three cloud seeding events carried out on 21 August, 23 August and 24 August in 2019, are selected here for evaluation of seeding signatures and plaussible links to microphysical properties. Instruments for the measurement of flare particles, aerosol, and cloud properties were operated on a Beechcraft-B200 aircraft. This aircraft was equipped with flare racks located under both the wings and the belly. The former were used for warm cloud seeding operations, while the latter were utilized for cold cloud seeding operations. The thermodynamical and meteorological parameters, such as temperature (T, ºC), relative humidity (RH%), wind speed (ms^{-1}) and directions were measured using the Airborne Integrated Meteorological Measurement System (AIMMS-20) probe. The droplet size distribution (DSD) in the diameter (D) range of 2-50 µm was measured with a Cloud Droplet Probe (CDP-2) manufactured by Droplet Measurement Technologies LLC, USA. The bulk microphysical properties are derived from the measured DSDs, e.g. the total number concentration (N_t, cm^{-3}) and liquid water content (LWC, g m^{-3}). The values of effective radius (r_e, µm) were calculated from the ratio between the third and second moments of the DSDs (Martin et al., 1994). The Precipitation Imaging Probe (PIP) was used to document drizzle drops in the clouds. The PIP measures DSDs in the diameter range of 100-6200 µm. The technical specifications of these instruments are shown in Table 1.

The cloud properties are altered by the entrainment of air masses near the periphery or the edges of the cloud. Therefore to minimise influences of entrainment and mixing processes in the

https://doi.org/10.5194/amt-2023-171
Preprint. Discussion started: 19 September 2023

seeded and non-seeded clouds, the near adiabatic or slightly diluted cloud parcels are considered to evaluate cloud microphysical properties. The mean DSDs are calculated from the slightly diluted cloud parcels. The slightly diluted DSDs falling within the liquid water content (LWC) range of $0.75 < LWC/LWC_{max} < 1$ (Konwar et al., 2021) are considered. Here, LWC_{max} represents the maximum measured value of LWC during a cloud pass. Further, the DSDs for Seed Cloud (SCl) and No Seed Cloud (NSCl) conditions are compared at different cloud depths (CD, km), where CD is defined as the distance from the cloud base to the measured cloud height. The lowest unbroken visible section of a convective cloud was selected as the cloud base. The cloud top is defined as the maximum altitude attained by these clouds at any given moment.

https://doi.org/10.5194/amt-2023-171
Preprint. Discussion started: 19 September 2023

Atmospheric Measurement Techniques Discussions

Table 1

Details of Instruments used on the aircraft and for offline analysis in the study

Instrument	Variable	Range/Remark	Reference
Aventech AIMMS-20	GPS Coordinates, altitude above Mean Sea Level (MSL), temperature, dew point temperature, horizontal and vertical winds	Vertical wind accuracy 0.75 m s^{-1}	https://aventech.com/products/aimms20.html
DMT CDP2	Cloud droplet number concentration and size distribution	3.0 – 50.0 µm	https://www.dropletmeasurement.com/product/cloud-droplet-probe/
DMT PIP	Particle image	100 µm – 6.2 mm	https://www.dropletmeasurement.com/product/precipitation-imaging-probe/
CVI	Allow residual particle of cloud to measure	Particle Cut size ~ 7µm	https://www.brechtel.com/product/aircraft-based-counterflow-virtual-impactor-inlet-system-cvi/

https://doi.org/10.5194/amt-2023-171
Preprint. Discussion started: 19 September 2023

Atmospheric Measurement Techniques Discussions

2.2 Measurement of hygroscopic flare particles by mAMS and Correcting time trends of slow-vaporizing species

As mentioned earlier, we utilized a mAMS to analyze the chemical compositions of residual particles from cloud droplets, specifically to trace flare particles within the seed clouds. The CVI is manufactured by Brechtel Manufacturing Inc. (BMI, Model 1204, www.brechtel.com). The cloud droplets were first passed through a CVI inlet to obtain the residual droplets before being sampled by the mAMS. Through the use of inertial impaction, the CVI inlet segregates and samples cloud elements. A warm dry nitrogen gas, free from particles, is pumped towards the inlet tip against the direction of the air flow. This causes a division in the incoming free stream air, with larger particles (D>7μm) in the sampled air exhibiting enough inertia to penetrate the counterflow and join the sample flow. The heated air leads to the evaporation of the cloud droplets. The dried cloud residuals (or nuclei) then enter the mAMS and their chemical compositions are classified. Details of operational principle of CVI inlet can be found in Ogren et al., 1985; Ogren, 1987; Noone et al., 1988; Shingler et al., 2012; Golderger et al. 2020; and references therein. Note that, since our main focus is on detecting the chemical traces of cloud seeding materials, we did not apply corrections such as transmission efficiency of CVI (Shingler et al., 2012) to the data analyzed by the mAMS.

An mAMS, onboard the research aircraft, measured in-situ aerosols with a vacuum aerodynamic diameter of less than 1 μm. The mAMS sampled through an aerodynamic lens. The aerosol sample stream was intermittently blocked to measure background signals. The aerosol signal was the difference between unblocked ("open") measurements and those obtained during the blocked ("closed") period. The AMS sampled 10 seconds of closed signal for every 110 seconds of open. The heater, operated at 600 ^{o}C, vaporized the sample, electron impact ionized the vapors, and the resultant ions were extracted into the mass analyzer for measurement of chemical composition and

https://doi.org/10.5194/amt-2023-171
Preprint. Discussion started: 19 September 2023

Atmospheric Measurement Techniques Discussions

mass distributions (Jayne et al., 2000; DeCarlo et al., 2006; Canagaratna, et al;, 2007; Drewnick et al., 2015; Giordano et al., 2018; Salcedo et al., 2006).

Ice Crystal Engineering (ICE) Inc. (USA) manufactured the hygroscopic flares used in this work. The flares were composed of an aggregated mixture of potassium perchlorate ($KClO_4$) and calcium chloride ($CaCl_2$) (Hindman, 1978; Bruintjes et al., 2012).

For non-refractory ambient aerosol species (i.e., NH_4, NO_3, SO_4) aerosol concentrations are obtained from the difference between the open and closed signals. The vaporization of non-refractory aerosol species at 600°C typically completes on the timescale of hundreds of microseconds, however, semi-refractory species such as metals and salts may take minutes to completely vaporize (Canagaratna et al., 2007; Salcedo et al., 2006).

As discussed below, the Cl, HCl, and K from the $KClO_4$ and $CaCl_2$ in flares is a semi-refractory species which exhibits slow vaporization. These slow vaporizing species were analyzed using only the open signals.The background signal was calculated from measurements obtained immediately before the cloud intercept of interest.

https://doi.org/10.5194/amt-2023-171
Preprint. Discussion started: 19 September 2023

Atmospheric Measurement Techniques
Discussions

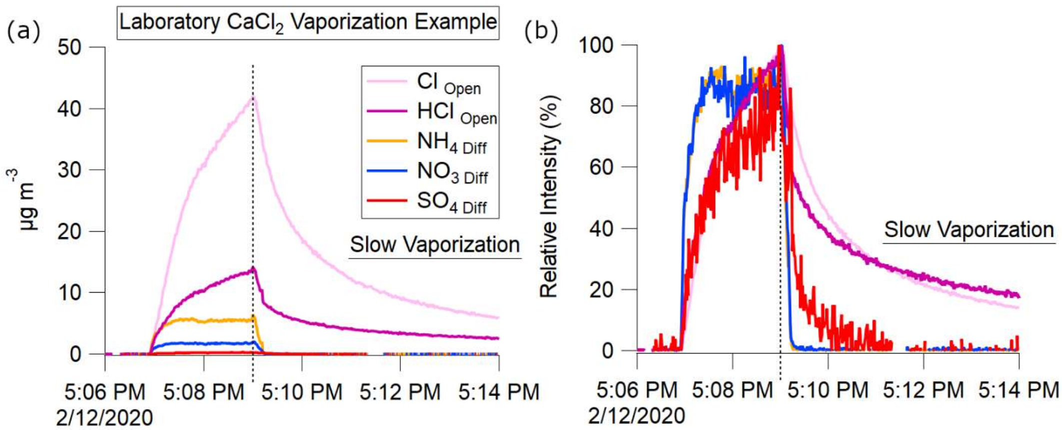

Figure 1. Laboratory atomized $CaCl_2$ AMS measurements observing slow vaporization of semi-refractory Cl species on 2/12/2020. Atomization begins at 5:07 PM ending at 5:09 PM. Slow vaporization is evident after 5:10 PM. The presence of NO_3, NH_4, and SO_4 are from calibration species (NH_4NO_3, NH_4SO_4) contaminants in the atomizer.

$CaCl_2$, the seeding component in the flares, has a melting point of 774 ºC. Laboratory measurements of atomized $CaCl_2$, primarily detected as Cl and HCl ions, exhibit the same slow vaporization seen in refractory salts (Drewnick et al., 2015). Fig. 1 shows a comparison of vaporization timescales of $CaCl_2$, NH_4NO_3, and $(NH_4)_2SO_4$ obtained with an AMS during laboratory measurements of $CaCl_2$ in solution with H_2O which had been atomized and passed through a drier before sampling. This behavior differs from that observed from non-refractory NH_4NO_3 and $(NH_4)_2SO_4$, which were present as tracers.

https://doi.org/10.5194/amt-2023-171
Preprint. Discussion started: 19 September 2023

Atmospheric Measurement Techniques
Discussions

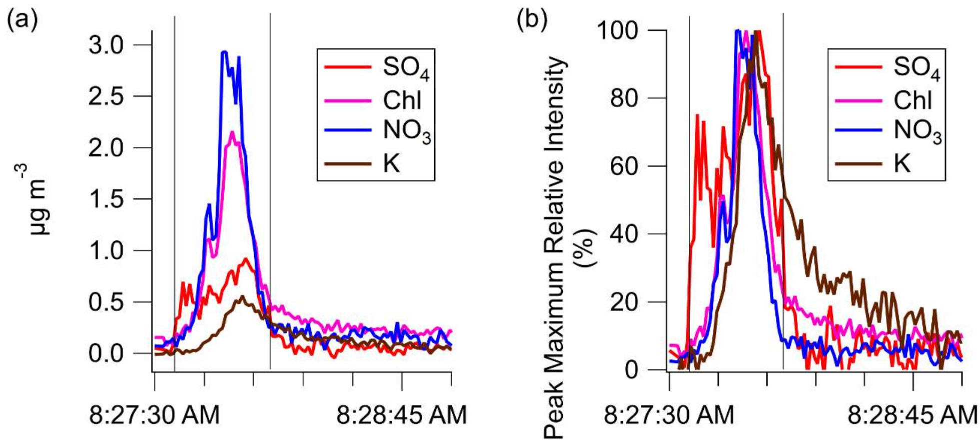

Figure 2. (a) shows the slowed time response of thespecies K and Cl for a seeded cloud pass on August 23rd (b) the relative intensity with respect to peak maximum of each species highlights the slowed decay of K and Chl compared to SO_4 or NO_3.

The seeded cloud pass shown in Fig. 2a exhibits a single seeded cloud pass. The K and Cl time series have a delayed decay to background compared to sulfate or nitrate. The relative intensity shown in Fig. 2b highlights the delayed response in thedecay of the two flare associated species (K, Cl).

An exponential decay was fit to each cloud intercept, from the signal peak to 5 e-folding times. The average decay exponential(τ) for Cl, and K across all seeded cloud intercepts, is shown in Table 2.

https://doi.org/10.5194/amt-2023-171
Preprint. Discussion started: 19 September 2023

Atmospheric Measurement Techniques Discussions

Table 2

Average decay time constants from seeded cloud intercepts during CAIPEEX- IV, 23 August 2019.

T	K	HCl	Cl
Mean	6.7	3.4	3.3
Std Dev	2.3	0.5	0.8

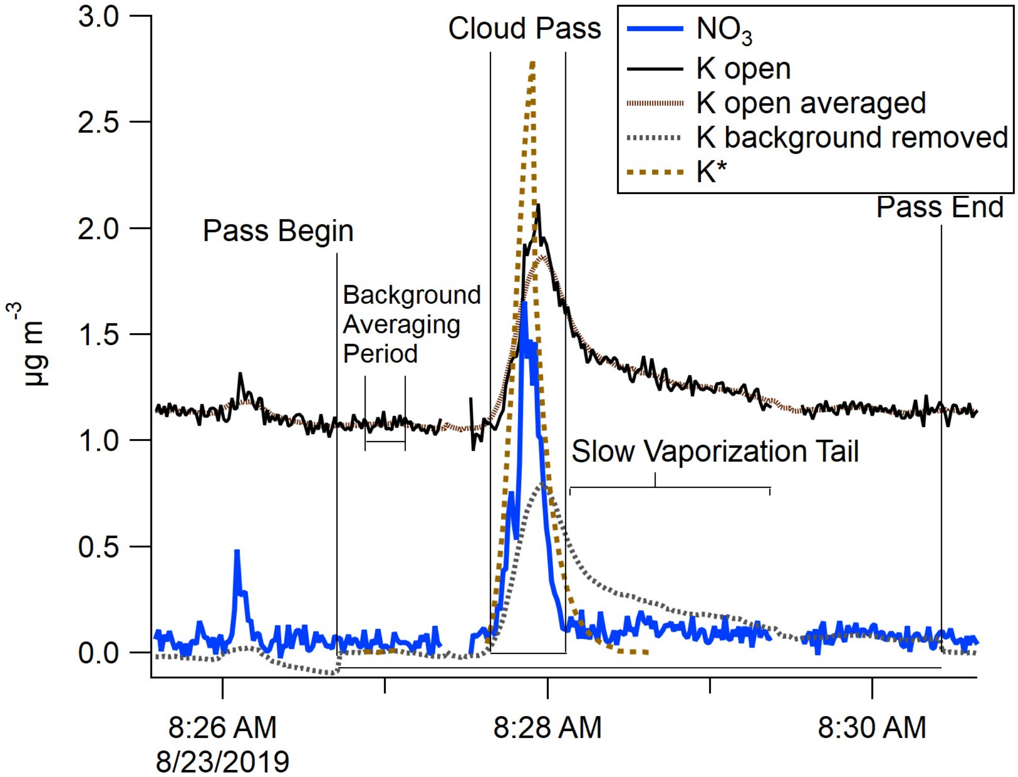

Figure 3. The measured semi-refractory open K signal and corrected K* signal from the mAMS are depicted for a seeded cloud pass on 23 August 2019. The periods for the start, peak, end, and tail of the pass are shown.

https://doi.org/10.5194/amt-2023-171
Preprint. Discussion started: 19 September 2023

Atmospheric Measurement Techniques Discussions
Open Access
EGU

For each slowly vaporizing species, a new corrected time series was created. The start, stop, and maximum total mass times were identified for each cloud pass (Fig. 3). For each species, a background signal was determined from measurements during the non-cloud period preceding each pass. This background was subtracted from the signal observed during each cloud intercept.

The cloud intercept time series peakat the same time as the uncorrected series. However, the tails were corrected to decay within 5 tau e-folding times, while preserving the total mass. The equations used in these calculations are shown below.

The measured mass from the start of the pass to the end of the slow vaporization regime was scaled by the ratio of the total area divided by the area of fast vaporization (equation 1)

$$Conc._{Areacorrected}(t)\Big|_{End+(5\tau)}^{Start} = (Conc.(t) - Conc._{Background}) * \frac{Area_{Peak+Tail}}{Area_{Peak}} \quad (1)$$

The decay of this normalized mass is adjusted to the exponential decay fit (Table 2) to the slow vaporized mass (equation 2). This decay extends from the cloud pass peak to the end of the normal vaporization period plus five e-folding times (Giordano et al., 2018)

$$Conc._{TailCorrected}(t)\Big|_{End+(5\tau)}^{Peak} = Conc._{AreaCorrected}(t) * e^{\left(-\left(\frac{1}{\tau}\right)t\right)} \quad (2)$$

This decay-corrected time-shifted time series is normalized to the unmodified slow vaporizing total mass (equation 3)

$$Conc._{Corrected}(t)\Big|_{End}^{Start} = Conc._{TailCorrected}(t) * \frac{Area_{Peak}}{Area_{Peak}+Area_{Peak+Tail}} \quad (3)$$

https://doi.org/10.5194/amt-2023-171
Preprint. Discussion started: 19 September 2023

Atmospheric Measurement Techniques Discussions

3. RESULTS

3.1.1 Slow vaporization of semi-refractory seed aerosols

The operational details of using the mAMS to identify non-refractory ambient aerosol species and semi-refractory aerosols are discussed in the materials and methods sections. As discussed, most aerosol species readily vaporize at 600 ^{o}C, some materials, semi-refractory in nature, do not. Cl, a major component of submicron aerosol in the troposphere is rarely semi-refractory and vaporizes quickly in the mAMS. However, Cl in seeded clouds was found to vaporize slowly. Cl measured from clouds seeded using $CaCl_2$ and $KClO_4$ exhibited the same slow vaporization (Fig. 2) as Atomized $CaCl_2$ in the laboratory (Fig 1). The majority of atmospheric Cl is non-refractory. In this work slowly vaporizing Cl was only observed in seeded clouds, thus we assume that slow vaporizing Cl was sourced from the flare material. Aerosol K is uncommon except as super micron mineral dust. As shown in Fig.2b, slowly vaporizing signals of Cl and K were observed in the campaign during seeded cloud intercepts.

The combination of the isolation of cloud droplets by the CVI inlet, the submicron diameter cutoff in the instrumentation, and the presence of K and semi-refractory Cl, allow for discrimination of the aerosol containing the flare combustion products.

Ca has a boiling point of over 1484 ^{o}C at ambient pressure. This high boiling point means this species was not vaporized inside the AMS and thus considered a refractory species. Since Ca could not be observed our study,the focus remained on the other species present.

As previously discussed, the time series of semi-refractory Cl and K signals are corrected to account for the difference in decay response of slowly vaporizing species in the mAMS. Fig. 3 depicts the corrected (K*) and uncorrected semi-refractory K signals in mAMS measurements for a seeded

https://doi.org/10.5194/amt-2023-171
Preprint. Discussion started: 19 September 2023

Atmospheric Measurement Techniques
Discussions

cloud pass, defining the periods for the start, peak, end, and tail of the pass. Details for correcting the time trends of the slow-vaporizing species are presented in the methodology section. For the remainder of the manuscript, K and Cl will refer to the corrected signals.

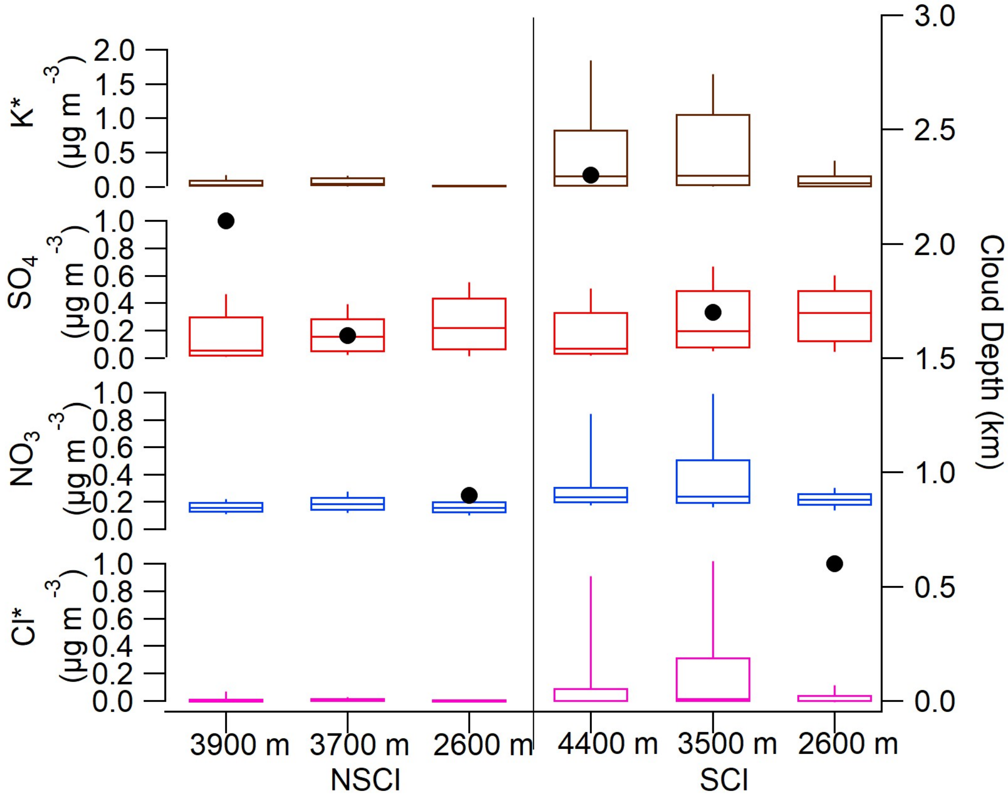

Figure 4. mAMS measurements of the mass density of Cl*, K*, NO_3, and SO_4 versus cloud depth (km) for cloud particle residuals on from six cloud passes through the same cloud on 23 August 2019. The vertical profile box plots of each mAMS species at different altitudes shows median

https://doi.org/10.5194/amt-2023-171
Preprint. Discussion started: 19 September 2023

Atmospheric Measurement Techniques Discussions

concentration and range (5-95%ile). Three passes are NSCI, then post seeding, three passes are SCI. The black dots indicate the cloud depths.

A vertical profile of cloud residual aerosols, within the same cloud, taken before and after seeding, provides a platform for measuring and observing cloud physical and chemical changes.The resultant mAMS measurements from one such experiment, on August 23, 2019, with three cloud passes of one cloudbefore and three after seeding are in Fig. 4.

All chemical species were found in higher quantities in the seeded cloud than in the non-seeded cloud. Cl and K concentrations were significantly increased for all seeded cloud passes above non-seeded cloud passes. The tracing of the chemical species of flare in the seeded cloud indicates that the mAMS could successfully identify the cloud droplets that consist of flare materials residuals.

An additional observation is the increased NO_3 and SO_4 concentration in the cloud drops of seeded clouds at upper heights. We hypothesized that the increased concentrations of these two chemical species could be linked with the activation of the flare particles and other organics while mixing with the naturally available NO_3 and SO_4 aerosols. The increased concentration of NO_3 in the seeded cloud may also be due to the presence of more LWC. The additional water drives nitric acid (HNO_3) from gas to liquid NO_3 (Wang and Laskin, 2014).

This example highlights the ability of the mAMS to identify flare associated species, by both increased concentration and time response, in order to confirm the presences of cloud seed aerosol and the active hydroscopic seeding of clouds.

https://doi.org/10.5194/amt-2023-171
Preprint. Discussion started: 19 September 2023

3.2 Seeding experiment, Seeding Signature, and Cloud properties

3.2.1. Case i: 21 August 2019. The flight pattern of the aircraft during a cloud seeding experiment conducted on 21 August 2019 in a warm stratus layer is shown in Fig. 5a. The objective was to identify the seeding materials as a tracer mechanism and record the cloud microphysical properties. The wind direction was north-westerly at an altitude of nearly 4.10 km with a mean wind speed of 7 ms^{-1}. Several cloud passes (T=5.14 ºC, H=4.39 km) were made through the stratus layer before the dispersal of seeding materials. Four hygroscopic flares were burned, two at a time inside the layer cloud, during 8:01-8:08 UTC at H=4.10 km. Weak vertical velocity (W=0.61±1.53 m s^{-1}) prevailed indicating that the flares might have drifted horizontally. Repeated crosswind cloud passes at a similar level (T= 6.44 ºC, H= 4.10 km) were made along the downwind direction. The position of the cloud was documented with the latitude and longitudinal data obtained in real-time from the Aircraft-Integrated Meteorological Measurement System (AIMMS, https://aventech.com/products/aimms20.html) probe. The base of the cloud was at ≈ 4 km, and the cloud properties are described with reference to the distance from this height which is the cloud depth (CD, km). Discussions on cloud probes and data analysis are given in the material and method section.

https://doi.org/10.5194/amt-2023-171
Preprint. Discussion started: 19 September 2023

Atmospheric Measurement Techniques
Open Access
EGU
Discussions

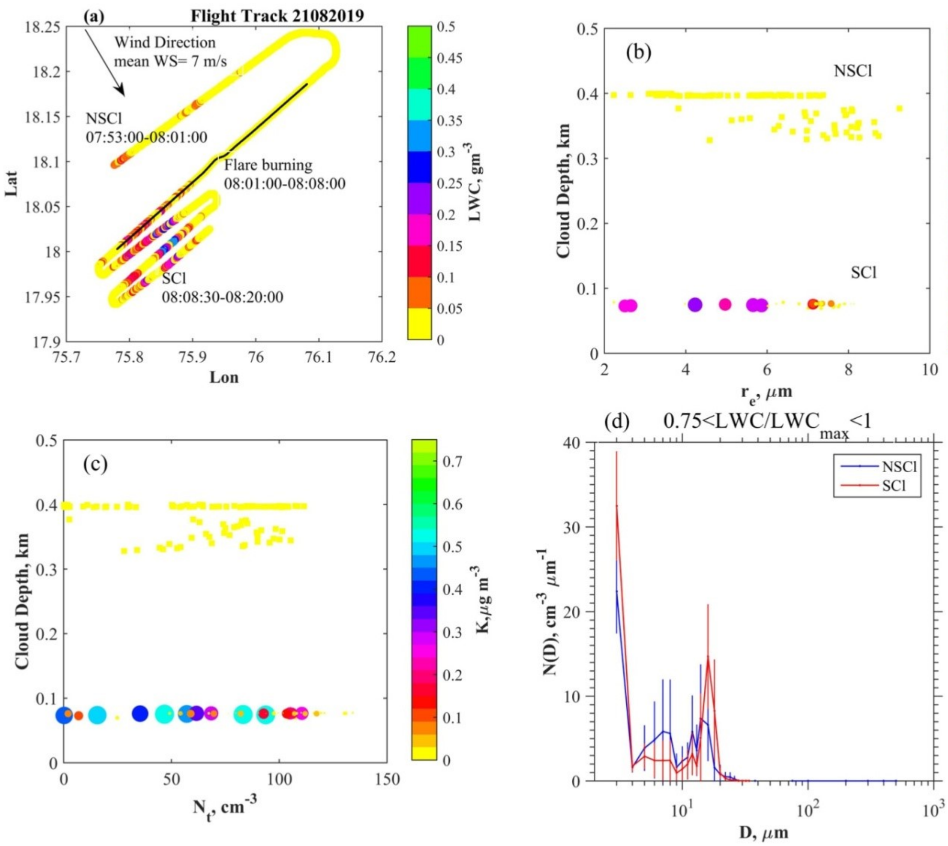

Figure 5. (a) Flight path during the seeding experiment on 21 August 2019. Liquid water content (LWC, gm^{-3}) at 1 Hz resolution is indicated. Periods during which cloud measurements were made for non-seeded cloud (NSCl) and seeded cloud (SCl) are indicated. The black line indicates the flare burning. Profiles of (b) N_t, cm^{-3} and (c) r_e , µm *w.r.t.* cloud depth (Km). The parameters are indicated with the mass densities of K, μmg^{-3} and Cl μmg^{-3}. (d) Mean cloud drop size distributions with standard deviations indicated by the error bars of slightly diluted clouds ($0.75<LWC/LWC_{max}$ <1) at various cloud depths, for NSCl and SCl.

After the dispersal of seeding materials enhanced quantities of K and Cl were observed in three cloud passes indicating the seeded clouds. Profiles of total cloud droplet concentrations (N_t, cm^{-3}) and effective radius (r_e, µm) with respect to (*w.r.t.*) CD are shown in Fig. 5(b,c), respectively. Mass concentrations of K and Cl are also indicated. The properties of DSDs along the cloud pass are shown in Supplementary Fig. S1 and S2. The DSD properties and mass concentrations of K and Cl are provided in Table 3. Increased droplet concentrations in the smallest size bin are noted after a few minutes from the seeding time. Drizzle drops were not formed in the SCl. Nearly adiabatic or slightly diluted SCl-DSD and NSCl-DSD are compared. Comparisons between NSCl-DSD and SCl-DSD are shown in Fig. 5d. An increase of N(D) at $D \approx 3$ µm and $13 < D < 20$ µm are noted in the SCl, while N(D) was decreased in the size range $4 < D < 13$ µm. The increase in the smallest cloud droplets may be due to freshly nucleated aerosols, probably due to the activation of seeding materials. The increase in the mid-size cloud droplet concentrations could be due to the collection of small-size cloud droplets by the mid-size droplets. Since drizzles were not formed, it may be suggested that hygroscopic seeding in stratus cloud with low LWC value e.g. < 0.5 g m^{-3} may not yield a significant positive seeding effect for the production of drizzle.

3.2.2 Case ii: 23 August 2019.

Fig. 6a depicts the flight patterns for the case on 23 August 2019. This seeding event is selected for evaluation because (i) The SCl and NSCl convective clouds were isolated, in the growing and non-precipitating stages, (ii) the cloud top was below freezing level (5 km); therefore ideal for studying warm rain microphysics, (iii) The SCl and NSCl were formed within the same area (20 X 20 km^2) and lastly, (iv) both the SCl and NSCl grew to similar cloud top altitudes (≈4 km), therefore roughly at similar growth stages. These conditions made this case suitable for seeding effect on warm rain.

https://doi.org/10.5194/amt-2023-171
Preprint. Discussion started: 19 September 2023

The cloud base height over the observational area was nearly 1.80 km. Northwesterly winds (mean wind speed of 12 ms^{-1}) prevailed in the boundary layer at 1.30 km (850 mb). Before the dispersal of flare materials below the convective cloud, the cloud microphysical properties of NSCl were measured from 7:49 to 8:06 UTC by step-wise multiple cloud penetrations from the top (≈ 3.90 km) to near the cloud base (≈ 1.80 km). A maximum updraft of 4.40 ms^{-1} was observed at the cloud base. After completion of NSCl measurements, the aircraft then circled below the cloud base and burned four hygroscopic flares (two on each wing) in the updrafts during 8:08-8:12 UTC. Then several step-wise cloud penetrations at nearly 1000 ft intervals were made, from near the cloud base to cloud-top during the period 8:14-8:28 UTC.

The profiles of N_t (cm^{-3}) and r_e (μm) *w.r.t.* the CDs are shown in Fig. 6(b,c). The mass densities of K and Cl corresponding to N_t and r_e, respectively, are also indicated. The statistical properties of the DSD parameters are presented in Table 3. The variations of DSDs along the cloud transects, values of r_e, drizzle concentration, LWC (gm^{-3}), and vertical velocity (W, ms^{-1}) are shown in the supplementary Fig. S3-4. The following differences in microphysical properties of SCl compared to NSCl were noted:

https://doi.org/10.5194/amt-2023-171
Preprint. Discussion started: 19 September 2023

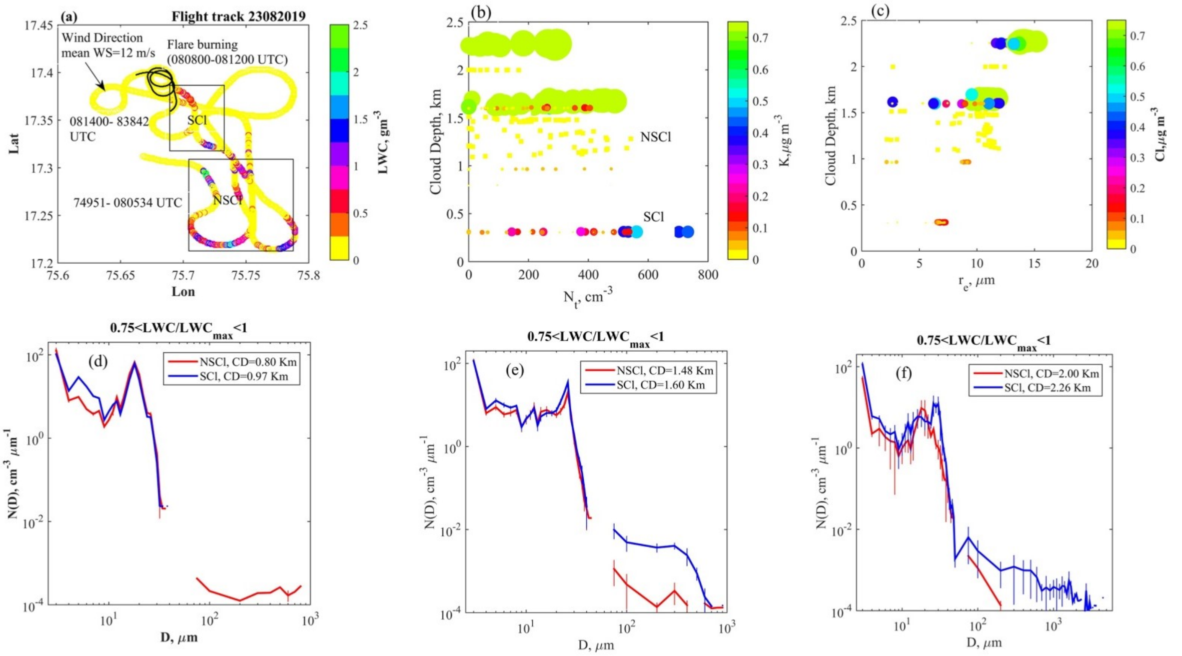

Figure 6. (a) Flight track during the seeding experiment on 23 August 2019. The flight track during the flare burning period is overlaid with black color. The areas of seeded cloud (SCl) and non-seeded cloud (NSCl) are indicated on the figure panels. The arrow indicates the wind direction near the cloud base height of 1.80 km. The color bar indicates the liquid water content (LWC, gm^{-3}) of clouds. Profiles of (b) N_t, (cm^{-3}) and (c) r_e, (μm) *w.r.t.* cloud depth (km). The parameters are indicated with the mass densities of K, μmg^{-3} . Mean cloud drop size distributions with standard deviations indicated by the error bars of slightly diluted clouds ($0.75<LWC/LWC_{max}<1$) at various cloud depths, for (d) NSCl and (e) SCl.

Table 3.

Cloud properties of Non-Seeded Cloud (NSCl) and Seeded Cloud (SCl) along the cloud transect are shown. Cloud depth (CD, km), Mean values and standard deviation of total droplet concentration N_t, (cm^{-3}) in the diameter range 2-50 µm, maximum droplet concentration (N_{tmax}, cm^{-3}), mean effective radius (r_e, µm), liquid water content (LWC, gm^{-3}), Maximum LWC (LWC_{max}), maximum adiabatic fraction (AF = LWC_{max}/LWC_{ad}), where LWC_{ad} is the adiabatic LWC calculated from a parcel model. AF for layer clouds on 21082019 is not calculated. The mean of small droplet concentration (D<11 µm) and the maximum of small droplet concentration, and drizzle concentration (DrizzleCon, (cm^{-3}) are also shown. Concentrations of K and Cl in $µgm^{-3}$ during NSCl and SCl observations are indicated. Due to limited field calibrations, the concentrations presented here are nitrate equivalent. Below Detection Limit (BDL) data are indicated.

Case	CD (km)	N_{tmn} ±SD (cm^{-3})	N_{tmax} (cm^{-3})	r_e ±SD (µm)	LWC ±SD (gm^{-3})	LWC $_{max}$ (gm^{-3})	AF	N_{tmn}, [N_{tmx}] (D<11µm)	DrizCon ±SD	K ±SD $µgm^{-3}$	Cl ±SD $µgm^{-3}$
2108-NSCl	0.40	31±26	65	3.34±0.20	0.003±0.003	0.01	-	31±26 [64]	0	BDL	BDL
2108-NSCl	0.40	73±35	111	5.93±1.03	0.05±0.03	0.13	-	39±20 [77]	0.004±0.02	BDL	BDL
2108-SCl	0.07	47±40	108	7±1.50	0.05±0.05	0.13	-	21±16 [49]	0±0	0.01±0.01	0.02±0.003
2108-SCl	0.08	62±40	111	6.05±1	0.05±0.04	0.10	-	42±28 [80]	0±0	0.34±0.15	0.14±0.11
2108-SCl	0.08	92±35	134	7.54±0.86	0.11±0.06	0.23	-	44±17 [79]	0±0	0.02±0.02	0.003±0.0.002
2308-NSCl	1.99	65±60	167	10.72±2.86	0.19±0.17	0.48	0.13	30±27 [68]	0±0	BDL	BDL
2308-NSCl	1.48	177±104	360	9.70±2.42	0.42±0.34	1.11	0.41	101±57 [185]	0.01±0.01	BDL	BDL
2308-NSCl	1.33	254±173	541	10.26±1.31	0.69±0.48	1.57	0.61	121±84 [262]	0.01±0.01	BDL	BDL
2308-NSCl	1.16	254±184	528	9.40±3.22	0.80±0.66	2.00	0.88	116±75 [210]	0.31±2.65	BDL	BDL
2308-NSCl	0.80	208±198	538	6.57±2.60	0.32±0.44	1.22	0.80	107±84 [221]	0.05±0.04	0.01±0.003	BDL
2308-SCl	0.31	402±194	733	6.74±0.84	0.42±0.22	0.69	0.92	144±69 [323]	0±0	0.18±0.14	0.09±0.05
2308-SCl	0.31	236±192	482	5.90±1.64	0.23±0.20	0.54	0.72	90±67 [169]	0±0	0.02±0.02	0.003±0.001
2308-SCl	0.96	186±158	477	7.30±3.01	0.35±0.31	0.97	0.51	81±71 [196]	0.002±0.007	0.03±0.01	0.06±0.02
2308-SCl	1.64	200±139	488	10.41±1.50	0.62±0.51	1.74	0.57	83±53 [198]	0.53±0.50	1.00±0.63	0.71±0.47
2308-SCl	1.60	162±120	332	9.70±3.00	0.50±0.38	1.04	0.34	71±54 [157]	0±0	0.02±0.01	0.02±0.01
2308-SCl	1.60	184±139	404	9.50±2.82	0.57±0.58	1.55	0.51	95±63 [183]	0.41±0.43	0.06±0.05	0.16±0.15
2308-SCl	2.26	175±107	320	13.10±1.14	0.80±0.50	1.49	0.38	83±51 [155]	0.43±0.52	1.25±0.85	0.77±0.67
2408-NSCl	0.21	92±92	244	5.55±1.76	0.06±0.06	0.18	0.31	56±59 [147]	0±0	BDL	0.01±0.01
2408-SCl	0.20	159±153	413	5.57±1.76	0.14±0.15	0.41	0.70	65±57 [157]	0±0	0.01±0.01	0.01±0.01
2408-SCl	0.20	161±189	649	5.91±2.06	0.16±0.18	0.56	0.96	70±88 [321]	0±0	0.07±0.05	0.03±0.02
2408-SCl	0.20	300±171	603	6.58±1.30	0.32±0.19	0.54	0.93	111±72 [347]	0±0	0.19±0.07	0.07±0.04

(i) After seeding, N_t (cm^{-3}) increased for SCl than NSCl at lower CD. An increase in the number concentration N(D) at D ≈14 µm is noted (Fig. S4a-e). Such enhancement in N(D) was not observed in the DSDs of NSCl (Fig. S3). At the deeper CD, N_t was decreased with increased r_e values, indicating an active CC process. (ii) At deeper CD ≈ 2.26 km, larger values of r_{eSCl} =13±1.14 µm for SCl are found. At a similar CD, i.e., 1.99 km, smaller values of r_{eNSCl} = 10.72±2.86 µm are found. The difference between r_e values at these CDs is significant above 95% confidence level. The large standard deviations in r_e values at different CDs indicated the mixing of dry air with the cloud volume. (iii) The mean DSDs are shown in Fig. 6(d,e) considering the slightly diluted clouds (i.e., 0.75< LWC/LWC_{max}< 1) of the cloud transects. Though r_e values were small for SCl at lower CD, some drizzle drops were already formed. The seeding effect may give rise to the initial production of drizzle particles, which were seen along the tail of the DSDs. Hence, the tail effect of the seeding particles has seemed to be active. Note that since the cloud passes were made in the developing stage of the cloud, these drizzle drops were formed spontaneously, not falling from the cloud tops because their terminal velocities are less than the updraft velocities. The broadening of the DSDs will serve to further increase the efficiency of the CC process (Andreae, et al, 2004; Rosenfeld et al., 2008; Rosenfeld et al., 1994; Freud et al., 2012; Konwar et al., 2012) leading to the production of drizzle drops at higher CDs. Also, stronger updrafts (≈ 5 ms^{-1}) were observed in SCl (see Fig. S4n), which helped in the growth of larger-size droplets.

(iv) The formation of drizzle drops (D>100 µm) in the SCl was noted (Fig. 6(e,f) and Fig. S4) while no significant drizzle concentrations were noticed for NSCl (Fig. S3). The difference in drizzle concentration suggests that the flare particles modulate the mid-size cloud droplets (D ≈ 14 µm) that grow further by diffusion and the collision and coalescence processes. As the drizzle drops fall under the influence of gravity, stronger downdrafts are most likely due to the cooling by evaporation (see

https://doi.org/10.5194/amt-2023-171
Preprint. Discussion started: 19 September 2023

Atmospheric Measurement Techniques Discussions

Fig. S4n). Moreover, small droplets of D≤11 μm were observed at high altitudes for both clouds (Table 3). The scatter plots between r_e -K and r_e-Cl are shown in Fig. S5. The prevailing dynamical conditions e.g., vertical velocity (W, ms^{-1}) are also indicated. It is found that the larger size droplets (greater r_e values) are associated with the larger mass densities of K and Cl, in the SCl. In both the updrafts and downdrafts, all these chemical species were present. The greater amount of the seeding materials in the downdrafts, with r_e >12 μm, are associated with the drizzle formation. Having found the seeding tracers Cl and K at different altitudes, it may be emphasized that the modification of cloud properties occurs due to the dispersal of seeding particles through the cloud base. Seeding particles were present at deeper CDs as the cloud droplets were transported through updrafts and re-circulated as the cloud developed (Khain et al., 2013).

It is important to note that the differences in cloud microphysical properties observed between the seeded and unseeded clouds could be a result of natural variability; however, given that these differences were accompanied by statistically different concentrations of chemical composition in the cloud droplet residues in the same environmental conditions, the evidence is compelling that seed material has a) transported to altitudes above the cloud base where they were released and b) these aerosol particles have influenced cloud microphysical processes.

3.2.3 Case iii: 24 August 2019.

The third cloud seeding case was carried out on an isolated convective cloud. The flight path is shown in Fig. **7**a. South-westerly winds with a mean speed of 9 m s^{-1} were noted near the cloud base at 2.1 km. A maximum updraft speed of 8 m s^{-1} was found. One cloud pass before the flare dispersal was made at 08:55-08:59 UTC above the cloud base at ≈ 2.3 km. Three downwind cloud passes during 09:05-09:07 UTC were made at ≈ 2.3 km after the flares were burnt. The variations of N_t (cm⁻

https://doi.org/10.5194/amt-2023-171
Preprint. Discussion started: 19 September 2023

Atmospheric Measurement Techniques Discussions

^{3}), and r_e (µm) *w.r.t.* cloud depths are shown in Fig. 7b,c . Increased concentrations of K and Cl are noted in SCl cases that identify the seeded clouds. The DSD properties of the clouds are shown in supplementary Fig. S6 & S7 and their parameters are indicated in Table 3. The mean DSDs (Fig. 7d) of slightly diluted clouds indicate increased droplet concentration in the small and mid-drop diameter ranges. This resulted in increased N_t after the seeding experiment. No marginal increment in r_e values was observed in the SCl.

https://doi.org/10.5194/amt-2023-171
Preprint. Discussion started: 19 September 2023

Atmospheric Measurement Techniques
Discussions

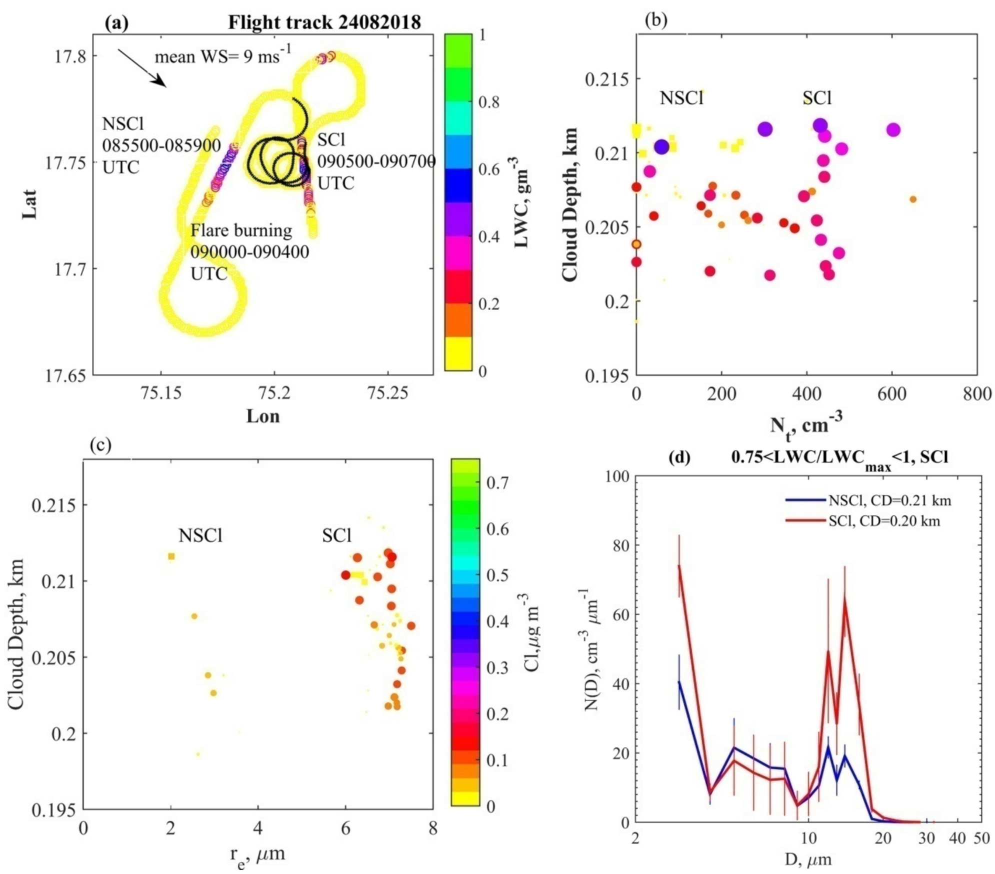

Figure 7. (a) Flight path during the seeding experiment on 24 August 2019. Periods during which cloud measurements were made for NSCl and SCl are indicated. The black line indicates the flare burning. Profiles of (b) N_t, (cm^{-3}) and (c) r_e, (μm) *w.r.t.* cloud depth (km). The parameters are indicated with the mass densities of K, ($\mu g m^{-3}$)' and Cl ($\mu g m^{-3}$). (d) Mean cloud drop size distributions with standard deviations indicated by the error bars of slightly diluted clouds ($0.75<LWC/LWC_{max}<1$) above the cloud base, for NSCl and SCl.

https://doi.org/10.5194/amt-2023-171
Preprint. Discussion started: 19 September 2023

4. DISCUSSIONS:

The successful identification of seeded cloud hydrometeors, and the tracing back to their seeding origins, in cloud seeding experiments, is an outstanding problem. The unequivocal identification of seeding material within clouds was the primary difficulty in such experiments. During CAIPEEX 2019 seeding experiments conducted in India, we measured cloud microphysical properties and traced the cloud flare seed material with an mAMS behind a CVI in convective and stratus clouds.

In the cloud seeding experiments, the mAMS identified an enhancement of both K and Cl, likely from the oxidizing agent (KClO) and seed material ($CaCl_2$) from the flares. In stratus and convective clouds, enhanced concentrations of refractory K and Cl should be considered as a seeding signature.

Increased small-size droplet concentrations near the cloud base of convective clouds and in a warm stratus layer are noted. This indicates that during monsoon season with available moisture supply, even small-sized CCNs present in the flares could be activated into cloud droplets.

In the case of a convective cloud, differences in the cloud microphysical properties of SCl compared to NSCl are noted. The flare materials released below the cloud base were propagated to a cloud depth of 2.25 km. In the lower part of the SCl larger droplet concentrations were noted. The SCl also had a larger r_e than the NSCl at similar cloud depths. The seeded clouds had more drizzle drops, suggesting that they reached the threshold for warm rain initiation at a lower distance from the cloud base than the non-seeded clouds.

This study identifies a novel methodology to simultaneously track and measure the cloud seeding signatures and to assess how the cloud seeding alters the microphysical properties of clouds leading to raindrop formation. The utilization of an mAMS in cloud seeding experiments together with a

https://doi.org/10.5194/amt-2023-171
Preprint. Discussion started: 19 September 2023

CVI allows for tracing the seeded cloud parcel of interest, leading to a better understanding of the effects on the microphysical properties of the cloud parcel. Although these measurements of flare material in seeded clouds are associated with changes in physical properties, the data set is too limited to unequivocally assert that this methodology will always be successful. Future studies with a much larger data set will provide more statistical evidence linking seed flare aerosol and increases in precipitation.

Acknowledgment: Indian Institute of Tropical Meteorology, Pune and the CAIPEEX project are funded by the Ministry of Earth Sciences, Govt. of India. We thank Director, IITM for continuous supports. The authors are grateful to the team members, the ground staff, V. Ruge and S. Patil of M/S Tesscorn AeroFluid, Inc., and the pilots for their dedicated efforts in conducting the project.

Data availability

mAMS and Cloud data are available at:
https://iitmcloud.tropmet.res.in/index.php/apps/files/?dir=/&fileid=59847#

Author contributions

TP and DW designed the mAMS experiment; MK, BW and ECF prepared the initial draft; KH, MK, BW, ECF, SC, SB, NM, MV, SJ and TP participated in the aircraft experiment; DB, TP, DW, DA, PM, MK, BW, ECF, MV, SC,SB and SAD reviewed the manuscript. All authors agree with the final version of the manuscript.

Competing interests

The contact author has declared that none of the authors has any competing interests.

References:

Andreae ,M. O., Rosenfeld, D., Artaxo, P., Costa, A. A., Frank, G. P., Longo, K. M., and Silva-Dias, M. A. F.: Smoking rain clouds over the Amazon, Science, 303, 1337–1342, 2004.

Bowen, E. G.: A new method of stimulating convective clouds to produce rain and hail, Quarterly Journal of Royal Meteorological Society, 78, 37–45,1952.

Bruintjes, R. T.: A review of cloud seeding experiments to enhance precipitation and some new prospects, Bulletin of the American Meteorological Society, 80, 805-820, 1999.

Bruintjes, R. T., Clark, T. L., and Hall, W. D.: The dispersion of tracer plumes in mountainous regions in central Arizona: Comparisons between observations and modeling results, Jounral of Applied Meteorology, 34, 971-988, 1995.

Bruintjes, R. T., Salazar, V., Semeniuk, T. A., Buseck, P., Breed, D. W., and Gunkelman, J.: Evaluation of Hygroscopic Cloud Seeding Flares, The Journal of Weather Modification, 44(1), 69–94. https://doi.org/10.54782/jwm.v44i1.85, 2012.

Canagaratna, M. R., Jayne, J.T., Jimenez, J.L., Allan, J.D., Alfarra, M.R., Zhang, Q., Onasch, T.B., Drewnick, F., Coe, H., Middlebrook, A., Delia, A., Williams, L.R., Trimborn, A.M., Northway, M.J., DeCarlo, P.F., Kolb, C.E., Davidovits, P. and Worsnop, D.R.: Chemical and microphysical characterization of ambient aerosols with the aerodyne aerosol mass spectrometer. Mass Spectrometer Reviews, 26, 185–222, 2007.

Cooper, W. A., Bruintjes, R. T. and Mather, G. K.: Calculations pertaining to hygroscopic seeding with flares, Journal of Applied Meteorology, 36, 1449-1469, 1997.

DeCarlo, P. F., Kimmel, J. R., Trimborn, A., Northway, M. J., Jayne, J. T., Aiken, A. C., Gonin, M., Fuhrer, K., Horvath, T., Docherty, K.S., Worsnop, D. R. and Jimenez, J. L.: Field-deployable, high-resolution, time-of-flight aerosol mass spectrometer. Analytical Chemistry*,* 78, 8281–8289, 2006.

Drewnick, F., Diesch, J. M., Faber, P., and Borrmann, S.: Aerosol mass spectrometry: particle–vaporizer interactions and their consequences for the measurements, *Atmospheric Measurement and Techn.,.* 8, 3811-3830, 2015.

Flossmann, A., Michael, M., Abshaev, A., Bruintjes R., Masataka, M., Prabhakaran T. and Zhanyu, Y.: Review of advances in precipitation enhancement research, Bulletin of the American Meteorological Society, 100, 1465–1480, 2019.

Freud, E. and Rosenfeld, D.: Linear relation between convective cloud drop number concentration and depth for rain initiation, J. Geophys. Res. Atmosphere, 117, D02207, 2012.

https://doi.org/10.5194/amt-2023-171
Preprint. Discussion started: 19 September 2023

French, J. R., Friedrich, K., Tessendorf, S. A., Rauber, R. M., Geerts, B., Rasmussen, R. M., Xue, L., Kunkel, M. L. and Blestrud, D. R.: Precipitation formation from orographic cloud seeding. Proceeding of National Academy of Scienmces, United States of America, 115, 1168–1173, 2018.

Ghate,V. P., Albrecht, B. A., Kollias, P., Jonsson, H. H. and Breed, D. W.: Cloud seeding as a technique for studying aerosol-cloud interactions in marine stratocumulus, Geophysical Research Letters, 34, L14807, 2007.

Giordano, M. R., Kalnajs, L. E., Goetz, J. D., Avery, A. M., Katz, E., May, N. W., Leemon, A., Mattson, C., Pratt, K. A., and DeCarlo, P. F.: The importance of blowing snow to halogen-containing aerosol in coastal Antarctica: influence of source region versus wind speed, Atmos. Chem. Phys., 18, 16689–16711, https://doi.org/10.5194/acp-18-16689-2018, 2018.

Golderger, L. A., Pekour, M. S., and Hubbe, J. M.: Counterflow Virtual Impactor (CVI) Inlet Aboard Aircraft (INLETCVI-AIR) Instrument Handbook, DOE/SC-ARM-TR-254, https://www.arm.gov > doe-sc-arm-tr-254, 2020.

Hindman ,E. E.: Water droplet fogs formed from pyrotechnically generated condensation nuclei, J. of Weather. Modif., 10, 77-96, 1978.

Hodnebrog, Ø., Etminan, M., Fuglestvedt, J. S., Marston, G., Myhre, G., Nielsen, C. J., Shine, K. P. and Wallington, T. J.: Global warming potentials and radiative efficiencies of halocarbons and related compounds: A comprehensive review, Review of Geophysics, 51, 300-378, 2013.

Jayne, J. T., Leard, D. C., Zhang, X., Davidovits, P., Smith, K. A., Kolb C. E., and Worsnop, D. R.: Development of an Aerosol Mass Spectrometer for Size and Composition Analysis of Submicron Particles, Aerosol Science and Technology, 33:1-2, 49-70, DOI: 10.1080/027868200410840, 2000.

Konwar, M., Maheskumar, R. S., Kulkarni, J. R., Freud, E., Goswami, B. N. and Rosenfeld, D.: Aerosol control on depth of warm rain in convective clouds, J. Geophys. Res., 117, D13204, 2012. doi:10.1029/2012JD017585.

Konwar, M., Prabhakaran, T., Khain, A. and Pinsky, M.: Cloud microphysical structure analysis based on high-resolution in-situ measurements, J. Atmospheric Sci., 78, 2265-2285, 2021.

Konwar, M., Malap, N., Hazra, A., Axisa, D., Prabhakaran, T., and Khain, A.: Measurement of Flare Size Distribution and Simulation of Seeding Effect with a Spectral Bin Parcel Model, Pure and Applied Geophysics, 180, 3019–3034, 2023, https://doi.org/10.1007/s00024- 023-03293-z.

Kuba, N., and Murakami, M.: Effect of hygroscopic seeding on warm rain clouds–numerical study using a hybrid cloud microphysical model, Atmos. Chem. Phys., 2010, *10*, 3335–3351.

Kulkarni, J. R., Maheshkumar, R. S., Morwal, S. B., Padma Kumari B., Konwar M., Deshpande C.G., Joshi R. R., Bhalwankar R.V., Pandithurai G., Safai P.D., Narkhedkar S.G, Dani K. K., Nath

A., Nair, S., Sapre, V.V, Puranik P.V., Kandalgaonkar S., Mujumdar V. R., Khaladkar R.M., Vijayakumar R., Thara P. and B. N.Goswami: The cloud aerosol interaction and precipitation enhancement experiment (CAIPEEX): Overview and preliminary results. Current Science, 12, 413-425, 2012.

Manton, M., Stone, R. C., Pepler, A., Collins, D. R., Bringi, V. N., Thurai, M., Turner, L. and McRae, D.: The Queensland Cloud Seeding Research Program, Bulletin of the American Meteorological Society, https://doi.org/10.1175/BAMS-D-11-00060.1,75–90, 2012.

Mather, G. K., Dixon, M. J. and de Jager, J. M.: Assessing the potential for rain augmentation—the Nelspruit randomized convective cloud seeding experiment, Journal of Applied Meteorology, 35, 1465-1482, 1996.

Mather, G. K., Terblanche, D. E., Steffens, F. E. and Fletcher, L.: Results of the South African cloud seeding experiments using hygroscopic flares, Journal of Applied Meteorology, 36, 1433-1447, 1997.

Ogren, J. A., Heintzenberg, J., and Charlson, R. J.: In-situ sampling of clouds with a droplet to aerosol converter. Geophys. Res. Lett., 121–124,12, 1985.

Ogren, J. A., Heintzenberg, J., and Charlson, R. J.: Virtual impactor. US Patent No. 4, 689,052, 1987.

Prabha, T. V., Khain, A., Maheshkumar, R. S., Pandithurai, G., Kulkarni, J. R., Konwar, M, and Goswami, B. N.: Microphysics of premonsoon and monsoon clouds as seen from *in situ* measurements during the Cloud Aerosol Interaction and Precipitation Enhancement Experiment (CAIPEEX), J. Atmos. Sci.,68, 1882–1901, 2011.

Ravishankara, A. R., Solomon, S., Turnipseed, A. A. and Warren, R. F.: Atmospheric lifetimes of long-lived halogenated species, Science, 259, 194-199, 1993.

Ray, E. A., Moore, F. L., Elkins, J. W., Rosenlof, K. H., Laube, J. C., Röckmann, T., Marsh, D. R. and Andrews, A. E.: Quantification of the sf6 lifetime based on mesospheric loss measured in the stratospheric polar vortex, Journal of Geophysical Research- Atmosphere, 122, 4626-4638, 2017.

Rosenfeld, D., Axisa, D., Woodley, W. and Lahav, R.: A quest for effective hygroscopic cloud seeding, Jounral of Applied Meteorology and Climatology, 49, 1548-1562, 2010.

Rosenfeld, D., Woodley, W. L., Axisa, D., Freud, E., Hudson, J. G., and Givati, A.: Aircraft measurements ofthe impacts of pollution aerosols on clouds and precipitation over the Sierra Nevada, J. Geophys. Res.,113, D15203,doi:10.1029/2007JD009544, 2008.

Rosenfeld, D., and Gutman, G.: Retrieving microphysical properties near the tops of potential rain clouds by multispectral analysis of AVHRR data, Atmospheric Res., 34, 259–283, 1994.

Ryan,B. F. and King, W. D.: A critical review of the Australian experience in cloud seeding, Bulletin of the American Meteorological Society, 78, 239-254, 1997.

Salcedo, D., Onasch, T. B., Dzepina, K., Canagaratna, M. R., Zhang, Q., Huffman, J. A., DeCarlo, P. F., Jayne, J. T., Mortimer, P., Worsnop, D. R., Kolb, C. E., Johnson, K. S., Zuberi, B., Marr, L. C., Volkamer, R., Molina, L. T., Molina, M. J., Cardenas, B., Bernabé, R. M., Márquez, C., Gaffney, J. S., Marley, N. A., Laskin, A., Shutthanandan, V., Xie, Y., Brune, W., Lesher, R., Shirley, T., and Jimenez, J. L.: Characterization of ambient aerosols in Mexico City during the MCMA-2003 campaign with Aerosol Mass Spectrometry: results from the CENICA Supersite, Atmos. Chem. Phys., 6, 925–946, https://doi.org/10.5194/acp-6-925-2006, 2006.

Noone, K. J., Ogren, J. A., Heintzenberg, J., Charlson, R. J., and Covert D. S.: Design and calibration of a counterflow virtual impactor for sampling of atmospheric fog and cloud droplets, Aerosol Science and Technology 8(3): 235–244, https://doi.org/10.1080/02786828808959186, 1988.

Segal, Y., Khain, A., Pinsky, M. and Rosenfeld, D.: Effects of hygroscopic seeding on raindrop formation as seen from simulations using a 2000-bin spectral cloud parcel model, Atmospheric Research, 71, 3-34, 2004.

Segal, Y., and Pinsky, M. and Khain, A.: The role of competition in raindrop formation. Atmospheric Research, 83, 106-118, 2007.

Shingler, T., Dey, S., Sorooshian, A., Brechtel, F. J., Wang, Z., Metcalf, A., Coggon, M., Mülmenstädt, J., Russell, L. M., Jonsson, H. H., and Seinfeld, J. H.: Characterisation and airborne deployment of a new counterflow virtual impactor inlet, Atmos. Meas. Tech., 5, 1259–1269, https://doi.org/10.5194/amt-5-1259-2012, 2012.

Silverman, B. A.: A critical assessment of hygroscopic seeding of convective clouds for rainfall enhancement, Bulletin of the American Meteorological Society, 84, 1219-1230, 2003.

Stith, J. L., Griffith, D. A., Lynn Rose, R., Flueck, J. A., Miller, Jr. J. R., and Smith, P. L.:

https://doi.org/10.5194/amt-2023-171
Preprint. Discussion started: 19 September 2023

Atmospheric Measurement Techniques Discussions

Aircraft observations of transport and diffusion in cumulus clouds, Jounral of Applied Meteorology and Climatology, 25, 1959-1970, 1986.

Stith, J. L., Detwiler, A. G., Reinking, R. F. and Smith, P. L.: Investigating transport, mixing, and the formation of ice in cumuli with gaseous tracer techniques, Atmpshreic Research, 25, 195-216, 1990.

Tessendorf, S. A.; Bruintjes, R. T., Weeks, C., Wilson, J. W., Knight, C. A., Roberts, R. D. , Peter, J. R., Collis, S., Buseck, P. R., Freney, E., Dixon, M., Pocernich, M., Ikeda, K., Axisa, D., Nelson, E., May, P. T., Richter, H., Piketh, S., Burger, R. P., Wilson, L., Siems, S. T.,

Wang, B. and Laskin, A.: Reactions between water-soluble organic acids and nitrates in atmospheric aerosols: Recycling of nitric acid and formation of organic salts. J. Geophys. Res., 119, 3335-3351, 2014.

Khain, A. P, Prabha, T. V., Benmoshe, N., Pandithurai, G. and Ovchinnikov, M.: The mechanism of first raindrops formation in deep convective clouds, J. Geophys. Res., 118, 9123-9140, 2013.

Martin, G. M., Johnson, D. W. and Spice, A.: The measurement and parameterisation of effective radius of droplets in warm stratocumulus clouds, J. Atmos. Sci., 51, 1823-1842, 1994.

WMO: Report on the WMO international workshop on hygroscopic seeding: Experimental results, physical processes, and research needs, WMP Rep 35, WMO/TD Rep 1006 36, 68pp, 2000.